Journal of Organometallic Chemistry 745-746 (2013) 439–453

Contents lists available at ScienceDirect

Journal of Organometallic Chemistry

journal homepage: www.elsevier.com/locate/jorganchem

Characterization and oxidative addition reactions of rhodium(I) carbonyl cupferrate diphenyl-2-pyridylphoshine complexes

Walter Purcell*, Jeanet Conradie*, Trevor T. Chiweshe, Johan A. Venter, Linette Twigge, Michael P. Coetzee

Department of Chemistry, University of the Free State, 205 Nelson Mandela Drive, Bloemfontein 9300, South Africa

ARTICLE INFO

Article history:
Received 29 July 2013
Accepted 20 August 2013

Keywords:
Rhodium(I)
Diphenyl-2-pyridylphoshine
Carbonyl
Oxidative addition
Ionic intermediate

ABSTRACT

The oxidative addition of CH_3I to the [Rh(cupf)(CO)(DPP)] complex (DPP = diphenyl-2-pyridylphoshine and cupf = *N*-nitroso-*N*-phenylhydroxylaminen) was kinetically investigated using UV/vis and infrared spectroscopy. The kinetics followed in chloroform, acetonitrile and acetone as solvents, indicated three different consecutive reactions. Firstly, a very fast reaction (intermediate formation, IM), secondly, a slower reaction with the formation of the Rh(III) alkyl complex ($5.0(1) \times 10^{-3}$ M^{-1} s^{-1} for acetonitrile at 20 °C) and thirdly a very slow formation of the Rh(III) acyl complex as final product with a rate constant of $2.9(6) \times 10^{-4}$ s^{-1}. The same oxidative addition reaction in ethyl acetate as solvent exhibited only two reactions. Firstly the Rh(III) alkyl formation ($1.03(3) \times 10^{-3}$ M^{-1} s^{-1}), which was five times slower than in the other solvents. Secondly, the Rh(III) acyl formation, which was masked by solvent IR stretching frequencies in the detection area. Rh(III) acyl, however, was isolated from ethyl acetate. There was no indication of intermediate formation with ethyl acetate. This apparent discrepancy between the rate and the mechanism for the same reaction prompted a DFT study to gain more insight into the reactants and products of the reaction, as well as to try and determine the geometry of the transition state. The DFT study predicted the formation of a linear transition state (TS), followed by the formation of the cationic five-coordinate $[Rh(cupf)(CO)(DPP)(CH_3)]^+$ intermediate with the CH_3 group in the apical position and with the iodide ion drifting away into the solvent sphere. This was in agreement with the experimental very fast first reaction. The experimentally observed difference in the rates and mechanisms of the [Rh(cupf)(CO)(DPP)] + CH_3I reaction in ethyl acetate relative to the other solvents can be attributed to the rate of the formation and/or the build-up and conversion of the I.M.

1. Introduction

Rhodium catalysts exhibit scope and versatility that are probably unmatched by any other metal in industry today. The importance of catalysis to the chemical industry (€12 billion worth) is illustrated by a 2006-estimate that more than 95% of chemical products by volume are based on catalytic technologies [1]. More than 70% of all consumer products are based on catalytic processes and 20% of the world economy is directly or indirectly related to catalysis. Economic and environmental considerations are mainly the compelling reasons for the widespread use of catalysis. These processes normally introduce lower operating costs, higher purity and yield products with fewer side-products [2]. Industrial catalytical processes encompass four major market sectors, namely fuel refining (22%), polymerization (21%), chemical production (27%), and environmental remediation (30%).

The use of different rhodium(II) complexes as chiral catalysts in the insertion of carbenes and nitrenes in drug synthesis results in fewer reaction steps and exceptional enantioselectivity [3]. An example is the synthesis of Ritalin which normally requires eight to nine synthetic steps which are reduced to two steps using the rhodium catalyst. Another article reports the use of a rhodium catalyst capable of producing hydrogen from a renewable fuel source in a commercially viable manner [4]. CORDIS [5] reports the success of a rhodium catalyst to produce 50 times more hydrogen from a feed gas containing 0.5% phenol over a broad temperature range when compared to its commercial nickel counterpart.

Rhodium (Monsanto) [6,7] and iridium (Cativa) [8] are the catalysts of choice in the production of acetic acid from methanol and accounts for over 60% of the worldwide production. Research has shown that the actual catalytic cycles of these two processes consist

* Corresponding authors. Fax: +27 (0) 865255382.
E-mail addresses: purcellw@ufs.ac.za (W. Purcell), conradj@ufs.ac.za (J. Conradie).

0022-328X/$ – see front matter © 2013 Elsevier B.V. All rights reserved.
http://dx.doi.org/10.1016/j.jorganchem.2013.08.037

of six different steps, including oxidative addition, 1,1-insertion or CO insertion, CO association and reductive elimination. Important prerequisites for these metal complexes to undergo oxidative addition include an unsaturated coordination sphere, the ability to undergo a two electron oxidation process (from +1 to +3) as well as non-bonding electron density on the metal center. The key to fundamental research on these kinds of catalytic cycles is the greater understanding of the relationships between activity and catalyst structure, as well as ways to better predict, understand and control catalyst molecular architecture [9].

Another group of rhodium(I) and iridium(I) complexes, namely [M(LL′)(CO)(LX_3)] (where M = Rh(I) or Ir(I), LL′ = mono ionic bidentate ligands and LX_3 = different phosphines, phosphites, arsines and stibines) were identified as possible candidates for catalysis or model complexes to investigate all the possible parameters that influence oxidative addition reactions due to their adherence to the above-mentioned criteria for oxidative addition reactions. Numerous structural and kinetic studies [10a–p] were undertaken to investigate factors that influence the nucleophilicity of the metal centers, solvent interactions and steric bulk on the rate of oxidative addition, CO insertion and mechanistic elucidation. Additionally, diphenyl-2-pyridylphoshine (DPP) has the ability to not only coordinate to the metal center with the phosphorous atom [11a–d], but in some cases also with the pyridinium nitrogen, making the phosphine ligand a potential bidentate ligand [12a–c]. The increase in electron density due to the presence of a nitrogen atom in the phosphine also has the potential to alter the Lewis basicity of the phosphine and ultimately influence the oxidative addition reactions for the metal complexes. With this in mind the [Rh(cupf)(CO)(DPP)] complex (Hcupf = *N*-nitroso-*N*-phenylhydroxylamine) was prepared and the mode of bonding as well the phosphine's effect on the oxidative addition of methyl iodide to these complexes was investigated.

2. Experimental

2.1. General considerations

All chemicals were of reagent grade and were used without further purification. The $RhCl_3.3H_2O$ and diphenyl-2-pyridyl phosphine were purchased from Sigma–Aldrich. Solvents were purified and dried according to standard procedures prior to use. IR spectra were recorded with a Digilab FTS 2000 spectrometer while NMR data were obtained at 293 K with Bruker 300 and 600 MHz spectrometers. For characterization of the Rh(III) alkyl and acyl species, [Rh(cupf)(CO)(DPP)] (5 mg, 0.0101 mmol) was dissolved in 0.7 ml $CDCl_3$ and transferred to a 5 mm diameter NMR tube. Methyl iodide (10.0 μl) was added and a series of ^{1}H and ^{31}P NMR spectra were recorded for 30 h. A Varian Cary 50 spectrophotometer, equipped with a temperature controlled cell changer (accuracy ± 0.1 °C) was use for UV/visible measurements. A cell with NaCl windows was used to follow the IR kinetics. Elemental analyses were performed on a LECO Truspec Micro analyzer.

A Shimadzu ICPS-7510 ICP-OES with a radial-sequential plasma spectrometer was used for the wet chemical analysis of all the rhodium samples in the current study [13] using cobalt (228.616 nm) as internal standard. The vertically oriented ICP-OES with the 'radial viewing' plasma was found to be suitable due to its better detection limits compared to the axial viewing plasma. The wavelength at 343.489 nm was the most suitable since it was free from the spectral interference of the elements present in the sample. The rhodium standard (1000 ppm) was purchased from Aldrich Chemicals while analytical grade HCl (32%), HNO_3 (65%), as well as $Co(NO_3)_2.6H_2O$ were obtained from Merck Chemicals. Double distilled water was used for dilution and Schott Duran grade (A) type glassware was used during the metal analysis.

All the reactions were followed under pseudo-first-order conditions with the typical complex concentration of 2.5×10^{-4} M for the UV/visible measurements and 0.02 M for IR. The methyl iodide concentrations varied between 0.1 and 1.0 M. The observed first-order rate constants where calculated using a non-linear least-square program according to $At = A\infty + (A0 - A\infty)e^{-kobs.t}$ with At, A∞ and A0 the absorbance of the indicated species at time t, ∞ and 0 respectively [14]. Experimental values are presented by points and lines represent calculated values in the subsequent figures.

2.2. Synthesis

2.2.1. [Rh(cupf)(CO)$_2$] [15]

$RhCl_3 \cdot 3H_2O$ (0.5 g, 1.9 mmol) was dissolved in a few drops of water, added to 10 ml *N*,*N*-dimethylformamide (DMF), and refluxed to a yellow-orange color. The solution was cooled to room temperature before addition of *N*-nitroso-*N*-phenylhydroxylamine ammonium salt (cupf, 0.3 g, 1.9 mmol). Subsequently 100 ml cold water was added to the solution resulting in the suspension of a yellow product, which was removed by centrifuge and dried in a fume cupboard. The product was purified by dissolving it in 20 ml acetone, filtering using a micro-filtration technique, and drying at room temperature to obtain the final yellow powdered product. Yield: 70%. IR data: $\nu_{(CO)} = 2087, 2013\ cm^{-1}$. Elemental analysis of $RhO_4N_2C_8H_5$: (calculated values in brackets): C, 32.81 (32.45), H, 1.98 (1.71), N, 9.09 (9.46), Rh, 34.69 (34.76) %. ^{1}H NMR (300 MHz, $CDCl_3$, 20 °C): δ 7.89 (m, 3- & 5-H, cupf), 7.46–7.41 (m, 4H, 2- & 6H, cupf). $^{13}C\{^1H\}$ NMR (151 MHz, $CDCl_3$, 20 °C): δ 183.16 (d, $^1J_{Rh-C} = 74.9$ Hz, CO), 183.11 (d, $^1J_{Rh-C} = 72.8$ Hz, CO), 137.28 (s, 1-C, cupf), 129.90 (s, 4-C, cupf), 128.41 (s, 2- & 6-C, cupf), 119.63 (s, 3- & 5-C, cupf).

2.2.2. [Rh(cupf)(CO)(DPP)]

[Rh(cupf)(CO)$_2$] (0.2 g, 0.64 mmol) was dissolved in 10 ml methanol and the solution was slightly heated to 30 °C for 5 min to ensure homogeneity. Diphenyl-2-pyridylphosphine (0.2 g, 0.76 mmol) was added gently whilst stirring. The solution changed from yellow to red, and a yellow product precipitated immediately from the solution. The precipitate was removed by filtration, washed with methanol and dried in a fume cupboard. Yield: 60%. IR data: $\nu_{(CO)} = 1988\ cm^{-1}$. Elemental analysis of $RhPN_3O_3C_{24}H_{19}$: (calculated values in brackets): C, 54.0 (54.25), H, 3.73 (3.61), N, 8.20 (7.91), Rh, 19.16 (19.37) %. Two isomers were observed in the ^{31}P NMR spectra, with the minor isomer (isomer A) being 37.3% and the major isomer (isomer B) 62.7%, according to the ^{31}P resonance integrals. ^{1}H NMR (300 MHz, $CDCl_3$, 20 °C): δ 8.75 (m, 3-H pyridyl-ring, isomer A & B), 8.00 (m, 6-H pyridyl-ring, isomer A & B), 7.93 (m, 3- & 5-H cupf, isomer B), 7.75 (m, 2- & 6-H phenyl, isomer A & B), 7.68 (m, 5-H pyridyl-ring, isomer A & B), 7.47 (m, 3- & 5H cupf, isomer A), 7.44–7.20 (m, 4-H cupf, 4-H phenyl, 3- & 5-H phenyl, 4-H pyridyl-ring, 2- & 6-H cupf, isomer A & B). $^{13}C\{^1H\}$ NMR (151 MHz, $CDCl_3$, 20 °C) (Only major isomer B reported): δ 189.52 (dd, $^1J_{Rh-C} = 75.9$ Hz, $^2J_{P-C} = 25.3$ Hz, CO), 156.20 (d, $^1J_{P-C} = 74.4$ Hz, 1-C pyridyl-ring), 149.22 (d, $^3J_{P-C} = 14.7$ Hz, 3-C pyridyl-ring) 138.06 (s, 1-C, cupf), 134.87 (d, $^3J_{P-C} = 9.5$ Hz, 5-C pyridyl-ring), 133.55 (d, $^2J_{P-C} = 11.7$ Hz, 2- & 6-C phenyl), 131.11 (d, $^1J_{P-C} = 53.1$ Hz, 1-C phenyl), 129.95 (d, $^2J_{P-C} = 28.8$ Hz, 6-C pyridyl-ring), 129.63 (d, $^4J_{P-C} = 2.0$ Hz, 4-C phenyl), 128.09 (s, 4-C, cupf), 127.85 (s, 2- & 6-C, cupf), 127.17 (d, $^3J_{P-C} = 10.6$ Hz, 3- & 5-C phenyl), 123.10 (d, $^4J_{P-C} = 2.1$ Hz, 4-C pyridyl-ring), 118.75 (s, 3- & 5-C, cupf). $^{31}P\{^1H\}$ NMR (121 MHz, $CDCl_3$, 20 °C): δ 49.53 (d, $^1J_{Rh-P} = 176.2$ Hz, isomer A), 49.51 (d, $^1J_{Rh-P} = 171.1$ Hz, isomer B).

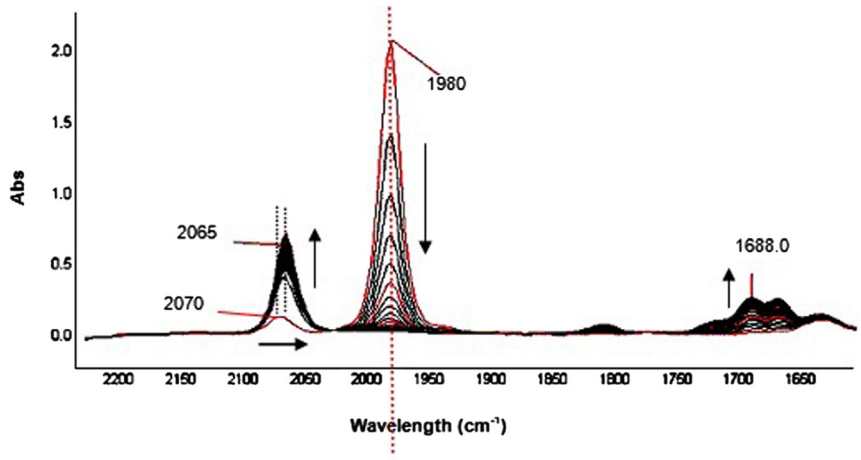

Fig. 1. IR spectra for the reaction of CH_3I (0.2 M) with [Rh(cupf)(CO)(DPP)] (2.0×10^{-2} M) in acetonitrile (2 min intervals, 25.0 °C).

2.2.3. [Rh(cupf)(CO)(DPP)(CH_3)I]

Methyl iodide (0.64 g, 4.55 mmol) was added to 5 ml chloroform solution containing [Rh(cupf)(CO)(DPP)] (0.25 g, 0.46 mmol). The reaction was allowed to proceed for 20 min at room temperature during which the color changed from orange to red brown. The solution was removed by evaporation to yield the dark brown powdered final product. Yield: 35%. IR data: $\nu_{(CO)} = 2061$ cm^{-1}. Elemental analysis of $RhIPN_3O_3C_{25}H_{22}$: (calculated values in brackets): C, 45.10 (44.60), H, 3.56 (3.30), N, 6.42 (6.24), Rh, 15.51 (15.28) %. Four isomers were observed. A ^{1}H–^{31}P HMBC experiment was used to assign the relevant ^{1}H and ^{31}P resonances. ^{1}H NMR (300 MHz, $CDCl_3$, 20 °C): δ 9.02–7.27 (cupf, pyridyl-ring, phenyl, 4 isomers), 2.06 (dd, $^2J_{Rh\text{-}H} = 2.0$ Hz, $^3J_{P\text{-}H} = 3.7$ Hz, Rh–CH_3, alkyl 2 – isomer A), 1.89 (dd, $^2J_{Rh\text{-}H} = 2.0$ Hz, $^3J_{P\text{-}H} = 3.7$ Hz, Rh–CH_3, alkyl 2 – isomer B), 1.32 (dd, $^2J_{Rh\text{-}H} = 2.0$ Hz, $^3J_{P\text{-}H} = 2.0$ Hz, Rh–CH_3, alkyl 1 – isomer B), 1.31 (dd, $^2J_{Rh\text{-}H} = 2.0$ Hz, $^3J_{P\text{-}H} = 2.0$ Hz, Rh–CH_3, alkyl 1 – isomer A). ^{31}P{^{1}H} NMR (121 MHz, $CDCl_3$, 20 °C): δ 41.67 (d, $^1J_{Rh\text{-}P} = 122.3$ Hz, alkyl 1 – isomer B), 41.17 (d, $^1J_{Rh\text{-}P} = 126.5$ Hz, alkyl 1 – isomer A), 32.88 (d, $^1J_{Rh\text{-}P} = 120.5$ Hz, alkyl 2 – isomer B), δ 30.04 (d, $^1J_{Rh\text{-}P} = 123.5$ Hz, alkyl 2 – isomer A).

2.2.4. [Rh(cupf)($COCH_3$)(DPP)I]

Methyl iodide (0.76 g, 4.55 mmol) was added to 5 ml ethyl acetate solution containing [Rh(cupf)(CO)(DPP)] (0.19 g, 0.44 mmol). The reaction was allowed to proceed for 500 min at room temperature during which the color changed from orange to red brown. The solution was removed by evaporation to yield a brown powdered final product. Yield: 20%. IR data: $\nu_{(COCH3)} = 1688$ cm^{-1}. Elemental analysis of $RhIPN_3O_3C_{25}H_{22}$: (calculated values in brackets): C, 45.65 (44.60), H, 3.37 (3.30), N, 6.38 (6.24), Rh, 16.35 (15,28) %. Two isomers were observed. ^{1}H NMR (300 MHz, $CDCl_3$, 20 °C): δ 9.02–7.27 (cupf, pyridyl-ring, phenyl, 2 isomers), 3.05 (broad singlet, Rh–$COCH_3$, acyl a), 2.93 (broad singlet, Rh–$COCH_3$, acyl b). ^{31}P{^{1}H} NMR (121 MHz, $CDCl_3$, 20 °C): δ 32.75 (broad doublet, $^1J_{Rh\text{-}P} = 151.2$ Hz, acyl b). Acyl a was not observed in ^{31}P NMR.

3. Computational chemistry

Density functional theory (DFT) and calculations were carried out using the ADF (Amsterdam Density Functional) 2012 programme [16–18] with the GGA (Generalized Gradient Approximation) functional PW91 [19]. The TZP (Triple ζ polarized) basis set with a fine mesh for numerical integration, a spin-restricted formalism and full geometry optimization with tight convergence criteria, was used for minimum energy and transition state (TS) searches. Approximate structures of the TS have been determined with linear transit (LT) scans, with a constrained optimization along a chosen reaction coordinate, to sketch an approximate path over the TS between reactants and products. Numerical frequency analyses [20,21] where the frequencies are computed numerically by differentiation of energy gradients in slightly displaced geometries, have been performed to verify the TS geometries. A TS has one imaginary frequency. Finally, the TS was allowed to relax after displacing the atoms according to the reaction coordinate as determined by the eigenvectors. This gave the reactants (relax from minimum stretch of frequency gave rhodium(I) complex and CH_3I) and the products (relax from maximum stretch of frequency gave cationic five coordinated complex and I^-) respectively. Throughout, all calculations have been performed with no symmetry constraint (C_1) and all structures have been calculated as singlet states.

Zero point energy and thermal corrections (vibrational, rotational and translational) were made in the calculations of the thermal parameters. The enthalpy (H) and Gibbs energy (G) were calculated from Ref. [22]

$$U = E_{TBE} + E_{ZPE} + E_{IE}$$

$$H = U + RT(\text{gas phase}) \text{ or } H = U(\text{solution})$$

$$G = H - TS$$

where U is the total energy, E_{TBE} is the total bonding energy, E_{ZPE} is the zero point energy, E_{IE} is the internal energy (sum of vibrational, rotational and translational energies), R is the gas constant, T is the temperature and S is the entropy. The entropy (S) was calculated from the temperature dependent partition function in ADF at 298.15 K. Solvent effects were taken into account for all calculations reported here. The COSMO (Conductor like Screening Model) model of solvation [23–25] was used as implemented [26] in ADF. The COSMO model is a dielectric model in which the solute molecule is embedded in a molecule-shaped cavity surrounded by a dielectric medium with a given dielectric constant (ε_0). The type of cavity used is Esurf [27] and The solvents used in the Conductor like Screening Model (COSMO) of solvation was methanol ($\varepsilon_0 = 32.6$), chloroform ($\varepsilon_0 = 4.8$), ethyl acetate ($\varepsilon_0 = 6.02$), acetonitrile ($\varepsilon_0 = 37.5$) and acetone ($\varepsilon_0 = 20.7$).

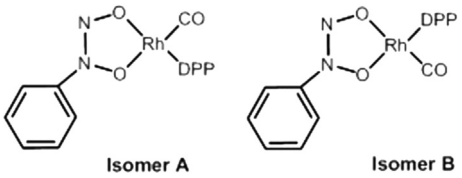

Fig. 2. The two possible [Rh(cupf)(CO)(DPP)] isomers.

4. Results

4.1. Synthesis and characterization of complexes

4.1.1. [Rh(cupf)(CO)$_2$] and [Rh(cupf)(CO)(DPP)]

A comparison between the IR spectra of the rhodium dicarbonyl complex and that of the substituted carbonyl complex shows the disappearance of one of the carbonyl stretching frequencies (2087, 2013 cm^{-1}). Thus, the displacement of one of the carbonyl ligands by the phosphine ligand with a shift to a lower wavelength of 1988 cm^{-1} for the mono substituted monocarbonyl complex is confirmed. This is in accordance with other complexes indicating an increase in electron density on the metal center, which can be attributed to the electronegativity of the phosphine and the absence of competition by the other carbonyl ligand. The decrease in ν(CO) indicates an increase in the metal-carbon π-back-bonding and a decrease in carbon–oxygen triple bond character.

4.1.2. [Rh(cupf)(CO)(DPP)(CH$_3$)I] and [Rh(cupf)(DPP)(COCH$_3$)I]

This dynamic process is also illustrated by the solvent IR in Fig. 1 with the disappearance of the monocarbonyl peak of Rh(I) at 1980 cm^{-1} (solid IR = 1988 cm^{-1}) with time and the formation of the Rh(III) alkyl peak at 2065 cm^{-1} (solid IR = 2061 cm^{-1}) and the Rh(III) acyl peak at 1688 cm^{-1} (solid IR = 1688 cm^{-1}). Isolation of the acyl complex is achieved by using ethyl acetate as solvent. The subsequent kinetic study indicates that the acyl formation reaction is much slower in this solvent compared to its formation in acetone, chloroform and acetonitrile and the alkyl was isolated with the quenching of the reaction just as the acyl began to form.

A comparison of the carbonyl stretching frequencies obtained in this study with those from other cupf complexes reveals interesting results. The carbonyl stretching frequency of [Rh(cupf)(CO)(DPP)] (this study and [28]) correlates well with that of the triphenylphoshine complex (1988 *vs* 1982 cm^{-1}) [10,29,30], but carbonyl stretching frequency of the oxidative addition product in the current study and [28] shifts slightly more (2061 *vs* 2052 cm^{-1}) [10], suggesting surprisingly less π-back-bonding in the current complex with its pyridyl-ring, compared to the triphenylphosphine complex.

4.1.3. Density functional theory (DFT) study of Rh(I) and Rh(III)-cupf complexes

The geometry of the most stable Rh(I) and Rh(III)-cupf complexes is presented using DFT results since no crystal structures are available for the complexes.

Square planar Rh(I) complexes: Two different isomers of the [Rh(cupf)(CO)(DPP)] reactant are possible, which are labeled Rh(I)-isomer A and Rh(I)-isomer B. For Rh(I)-isomer A, the DPP group is *cis* to the O nearest to the cupf-Ph group and for Rh(I)-isomer B, the DPP group is *trans* to the O nearest to the cupf-Ph group (Fig. 2). The DFT optimized geometries of the isomers in acetone as solvent are shown in Fig. 3. The population of the two isomers in selected solvents are shown in Table 1. Results indicate that the population of isomer A varies between 30 and 42%, depending on the solvent. It is well known that the two structural isomers of related [Rh(β-diketonato)(CO)(PR$_3$)] (PR$_3$ = tertiary phosphine of phosphite and if β-diketonato = unsymmetrical ligand) complexes exist in equilibrium and that the population ratio depends on the solvent and temperature [31–36]. Isomers isolated for structurally similar complexes, are controlled by the ligands bonded to the metal center as well as crystallization conditions [37]. Thus, isomer A crystallized in the solid state for [Rh(cupf)(CO)(PPh$_3$)], while isomer B was isolated for the [Rh(cupf)(CO)(P(OCH$_2$)$_3$CCH$_3$)] complex. The novel isolation of both isomers in same crystal structure was reported for [Rh(BA)(CO)(PPh$_3$)] (BA = benzoylacetylacetonato anion) [38] and [Rh(PhCOCHCO(CH$_2$)CH$_3$)(CO)(PPh$_3$)] [35]. For complex [Rh(PhCOCHCO(CH$_2$)$_3$CH$_3$)(CO)(PPh$_3$)] [39], both geometrical isomers crystallized in the same space in the unit cell at an 89.7:10.3 ratio. The two structural isomers of [Rh(cupf)(CO)(DPP)] in the current study are also experimentally observed in CDCl$_3$ with NMR spectroscopy in a 37.3:62.7% ratio, in excellent agreement with the calculated population of 37.0:63.0% in chloroform. The calculated geometry of isomer A and B for [Rh(cupf)(CO)(DPP)] is square planar, with bond lengths and angles similar to that found for the crystal structure of the related [Rh(β-diketonato)(CO)(PR$_3$)] complexes (Fig. 3).

Six coordinated Rh(III) alkyl complexes: The oxidative addition of iodomethane to [Rh(cupf)(CO)(DPP)] leads to a rhodium(III) alkyl product. The 12 possible rhodium(III) oxidative addition product isomers of the formula [Rh(cupf)(CO)(DPP)(CH$_3$)(I)], and calculated relative electronic energies of the optimized geometries (in acetone solvent) are displayed in Fig. 4. Two isomers result from trans addition of iodomethane and ten isomers result from *cis* addition or from the subsequent re-arrangement of a *trans* addition product. The energies indicate that four Rh(III)-alkyl isomers are significantly more stable than the others. These are the two *trans* alkyl product isomers (alkyl 1a and 2a) and the two alkyl isomers with DPP and I above and below the square plane through the two cupf-oxygens, CO and CH$_3$ (alkyl 2a and 2b). Alkyl 2a and 2b can be the products of *cis* addition or from re-arrangement of a *trans* addition product. The DFT results highlight that the barrier to *cis* addition is too high to be considered and that *trans* addition of iodomethane to [Rh(cupf)(CO)(DPP)] is energetically favored. The DFT calculations on the structurally similar rhodium-β-diketonato complexes, [Rh(β-diketonato)(CO)(PPh$_3$)] with β-diketone = 4,4,4-trifluoro^{-1}-(2-thenoyl)$^{-1}$,3-propanedione, 1-phenyl-3-(2-thenoyl)$^{-1}$,3-propanedione, 1,3-di(2-thenoyl)$^{-1}$,3-propanedione [40] 1-ferrocenyl-4,4,4-trifluorobutane^{-1},3-dione [33] or acetylacetone [41], is in agreement with experimental observations [10n,32], and also indicate *trans* addition of CH$_3$I to the square planar rhodium(I) complexes. The *trans* addition of iodomethane to the bisphosphite complex [Rh(CH$_3$COCHCOCH$_3$)(P(OPh)$_3$)$_2$], in agreement with ^{1}H NMR data [10f], is confirmed by a DFT computational study of the transition state and product of the oxidative addition reaction [42]. Although the crystal structure study of [Rh(cupf)(CO)(PPh$_3$)(CH$_3$)(I)] [10c] is similar to the alkyl 2a in this study, the computational results of the oxidative addition reaction of this study indicate that this structure is most probably due to the re-arrangement of the *trans* addition product as was experimentally found for the structurally similar [Rh(fctfa)(CO)(PPh$_3$)(CH$_3$)(I)] [10m] and [Rh(acac)(CO)(PPh$_3$)(CH$_3$)(I)] [40] complexes (Hfctfa = 1-ferrocenyl-4,4,4-trifluorobutane^{-1},3-dione and Hacac = 2,4-pentanedione (acetylacetone)). The optimized geometry of the *trans* [Rh(cupf)(CO)(DPP)(CH$_3$)(I)] alkyl product isomers is presented in Fig. 5.

When comparing the spin–spin coupling of the methyl protons of alkyl 1 and alkyl 2 with phosphorous (spin = 1/2; ^3J; ^{1}H–^{13}C–^{103}Rh–^{31}P), the values are 2.0 and 3.7 Hz respectively. This difference is due to the relative positions of the methyl and the phosphine ligands of Rh(III) alkyl 1 and Rh(III) alkyl 2 [41]. A ^3J value of 2 Hz and 4 Hz was previously found for the *trans* and *cis* alkyl products respectively for

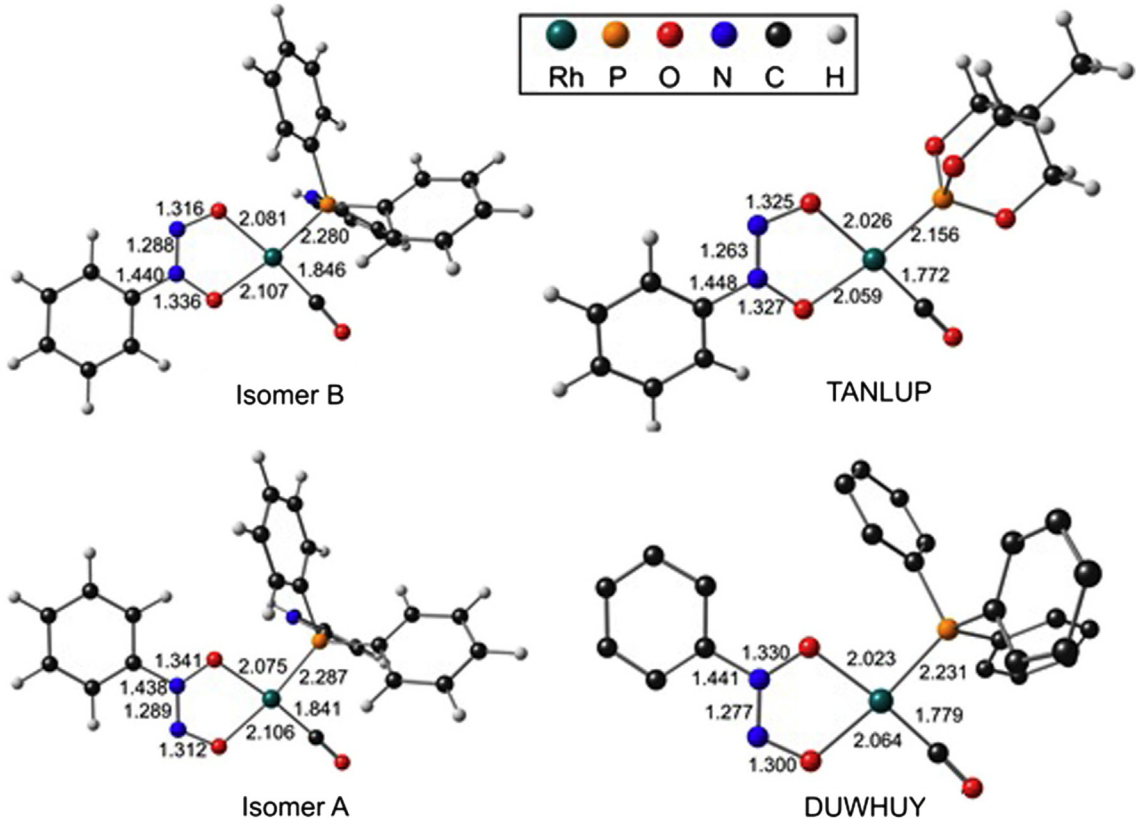

Fig. 3. The ADF/PW91/TZP/acetone optimized geometries of the two structural isomers of [Rh(cupf)(CO)(DPP)]. The experimental geometries of two Rh(cupf)(CO)(PR_3)] complexes that have been characterized by X-ray structures (CSD reference code shown) are shown for comparative purposes.

both [Rh(fctfa)(CO)(PPh_3)(CH_3)(I)] [10m] and [Rh(acac)(CO)(PPh_3)(CH_3)(I)] [41], consistent with the proposed geometry of the DFT calculated most stable alkyl isomers of this study (Fig. 4).

Five-coordinated Rh(III) acyl complexes: The CO insertion in a rhodium(III) alkyl moiety leads to a rhodium(III) acyl product. Fig. 4 gives the geometry and DFT calculated relative energies of the possible structural Rh(III) acyl isomers of the formula [Rh(cupf)(DPP)($COCH_3$)(I)]. The square pyramidal [Rh(cupf)(DPP)($COCH_3$)(I)] acyl products with the $COCH_3$ moiety in the apical position is the most stable (Fig. 6) for the optimized geometry. The energies of trigonal–bipyramidal geometries are too high or optimized to the square pyramidal geometry of acyl 2. The structurally similar [Rh(cupf)($P(OCH_2)_3CCH_3$)($COCH_3$)(I)] acyl, as well as all crystal structures of five-coordinated rhodium(III) acyl complexes [43] adopts a square pyramidal geometry with the $COCH_3$ moiety in the apical position [44]. Therefore, both computational calculations and crystallographic data are consistent with the geometry of the thermodynamic stable reaction product to be square-pyramidal with the $COCH_3$ group in the apical position. However, it is not possible to say if the observed acyl product is the final reaction product or only a reaction intermediate leading to the most stable acyl product.

4.2. Kinetic study

The reaction between [Rh(LL′)(CO)(DPP)] and CH_3I can be presented as follows:

$$[\mathrm{Rh(cupf)(CO)(DPP)}] + \mathrm{CH_3I} \rightarrow \mathrm{Products} \quad (1)$$

4.2.1. UV/vis spectra

The rate and type of reaction of oxidative addition between [Rh(cupf)(CO)(DPP)] and CH_3I was studied in four different

Table 1
ADF/PW91 calculated population of the optimized geometries of the two structural isomers of [Rh(cupf)(CO)(DPP)] in selected solvents. The energies of the transition state complex, the ionic intermediate and the *trans* Rh(III) alkyl product is also tabulated. The energy of the reactants is taken as 0.

Solvent	Rh(I)	Boltzmann population /%	E_{act}/kJmol^{-1} Linear TS(trans addition)	Bent TS	cis TS	E_{IM}/kJmol^{-1} Trans addition	E_{alkyl}/kJmol^{-1} Trans addition
Ethyl Acetate	Isomer-A	28.5	29	–	113	24	−34
	Isomer-B	71.5	28	–	–	25	−41
Acetone	Isomer-A	28.4	28	149	113	15	−33
	Isomer-B	71.6	27	149	–	22	−43
Chloroform	Isomer-A	37.0	30	–	113	26	−33
	Isomer-B	63.0	28	–	–	27	−42
Acetonitrile	Isomer-A	28.3	27	–	114	12	−32
	Isomer-B	71.7	28	–	–	20	−36
Methanol	Isomer-A	42.3	29	–	116	20	−31
	Isomer-B	57.7	28	–	–	21	−36

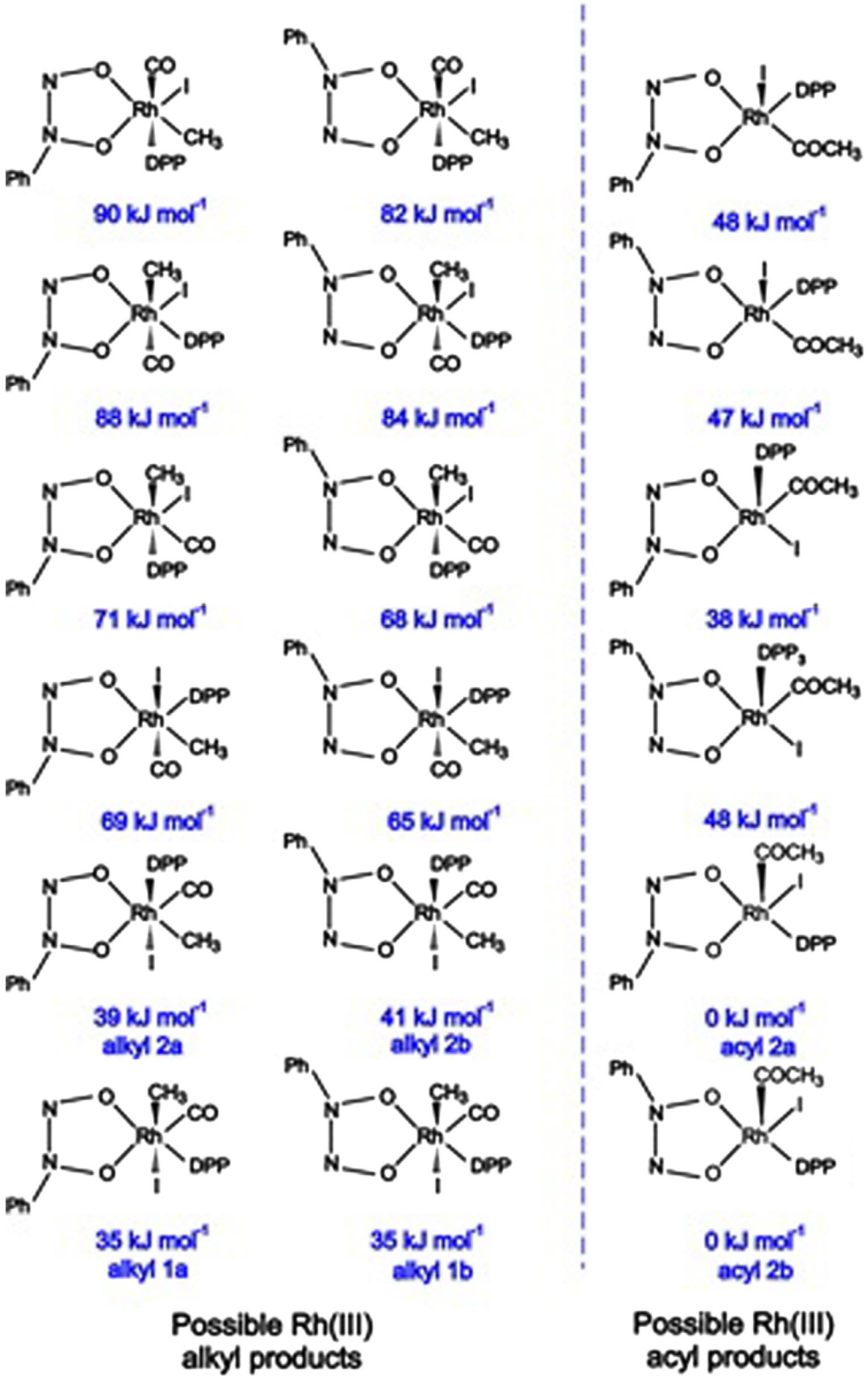

Fig. 4. Geometries and ADF/PW91/TZP/acetone calculated relative energies (ΔE_{TBE}) of the possible rhodium(III) alkyl and acyl products of the [Rh(cupf)(CO)(DPP)] + CH_3I reaction.

solvents. The addition of CH_3I to an acetonitrile solution containing [Rh(cupf)(CO)(DPP)] results in a change in the UV/visible spectrum. A relatively fast absorption increase and then a slow absorption decrease with the formation of an isosbestic point at 420 nm for the second reaction takes place (Fig. 7). This initial result indicates the existence of two possible reactions, with the second resulting in the formation of only one product. A time scan of the same reaction indicates the presence of two distinguishable reactions, with the first reaction (absorption increase) having $t_{½} = 110$ s and the second slower reaction (absorption decrease) with $t_{½} = 1400$ s (for

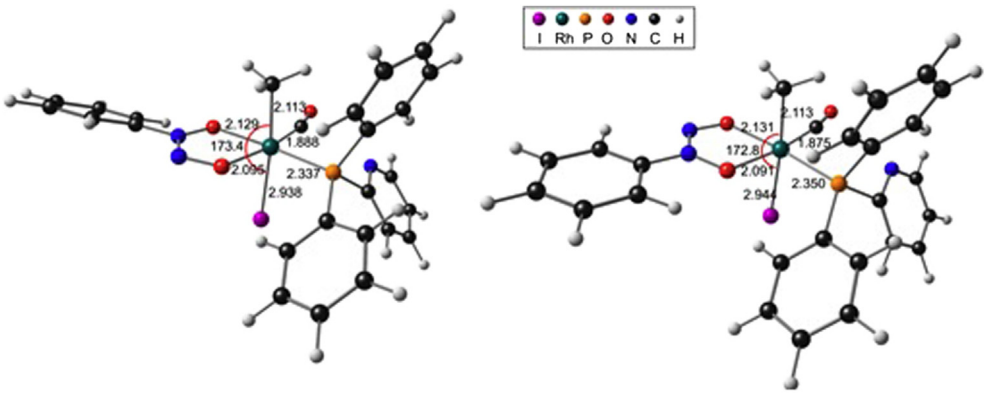

Fig. 5. ADF/PW91/TZP/acetone optimized geometry of the [Rh(cupf)(CO)(DPP)(CH_3)(I)] alkyl 1 product isomers that result from trans addition of CH_3I to [Rh(cupf)(CO)(DPP)].

[MeI] = 0.5 M). A time scan separation of the two reactions results in two distinguishable pseudo-first-order reactions. Similar results are obtained for acetone and chloroform with isosbestic points at 350 nm for both. Only one absorption change with $t_{½}$ = 3000 s (for [MeI] = 0.12 M) was observed for ethyl acetate using UV spectra before solvent evaporation made it impossible to further follow the reaction.

4.2.2. IR spectra

An IR study of the oxidative addition reaction between CH_3I and [Rh(cupf)(CO)(DPP)] in acetonitrile shows a fairly rapid disappearance of the Rh(I)—CO peak at 1980 cm^{-1} with the simultaneous appearance of the Rh(III)—CO stretching frequency at 2065 cm^{-1} (see Fig. 1). The same spectrum shows the slow appearance of the Rh(III)—$COCH_3$ peak at 1688 cm^{-1}. IR spectra for the same reaction in acetone and chloroform also shows the same disappearance of the Rh(I) peak and the formation of the Rh(III) alkyl peak. A comparison of the IR spectra, however, showed a substantially slower Rh(III) alkyl formation reaction in ethyl acetate compared to the other three solvents. Another important aspect of the IR spectra is the complete disappearance of the Rh(I)—CO peak.

Regarding reaction mechanisms, the IR spectra (Fig. 1) show that an absorption change in Rh(I) occurs immediately (first order change) with the addition of CH_3I, but the increase in Rh(III) only follows first order behavior between scans 1 and 2. The position of the peak maximum for the Rh(III) alkyl product changes from the initial 2070 cm^{-1} to 2065 cm^{-1}. Exactly the same behavior is evident for acetone and chloroform solvents. The absorption change observed during the formation of the Rh(III) alkyl product in ethyl acetate is much slower and shows first order behavior from the first scan with no detectable peak shift (Fig. 8). The large absorption maximum at 1680 cm^{-1} for ethyl acetate prevented the monitoring of the acyl product with IR spectra. However, product isolation from ethyl acetate solution after 500 min clearly indicated the $\nu_{(COCH3)}$ at 1688 cm^{-1}, confirming the formation of the acyl product in all the solvents that were investigated.

4.2.3. NMR study

The oxidative addition reaction between CH_3I and [Rh(cupf)(CO)(DPP)] in $CDCl_3$ at 21 °C was kinetically followed on the NMR to get more insight in the character of the reaction products formed (Fig. 9). The ^1H NMR spectra shows a fast decrease in the signals of the Rh(I) starting complex with the immediate formation of the two Rh(III) alkyl 1 isomers, identified by the overlapping signals at 1.32 and 1.31 ppm (see the Experimental section for the resonances). The rate of formation of the Rh(III) alkyl 1 isomers are in agreement with the experimental rates measured on the UV/vis in chloroform. The signals of the Rh(III) alkyl 1 isomers soon decrease at a rate of *ca* 0.0006 s^{-1}. Two Rh(III) acyl isomers, identified by the broad signals at 3.05 and 2.93 ppm, form at the same slower, [MeI] independent rate, 0.0006 s^{-1}, as the decrease in the Rh(III) alkyl 1 isomers signals. This rate is also the same as measured at 19.8 °C on UV/vis in chloroform.

4.3. Mechanism and rate constant

An important result from an initial IR kinetic study in acetonitrile at 25 °C (Fig. 1) is that the observed rate for the disappearance of the Rh(I) complex ($t_{½}$ ~ 232 s) and the appearance of the Rh(III) alkyl complex ($t_{½}$ ~ 224 s) are within experimental error the same, while the appearance of the Rh(III) acyl is much slower with $t_{½}$ ~ 1136 s. The first reaction between CH_3I and [Rh(cupf)(CO)(DPP)] was also studied under similar conditions using UV/visible and IR in acetonitrile to try and identify or allocate the two

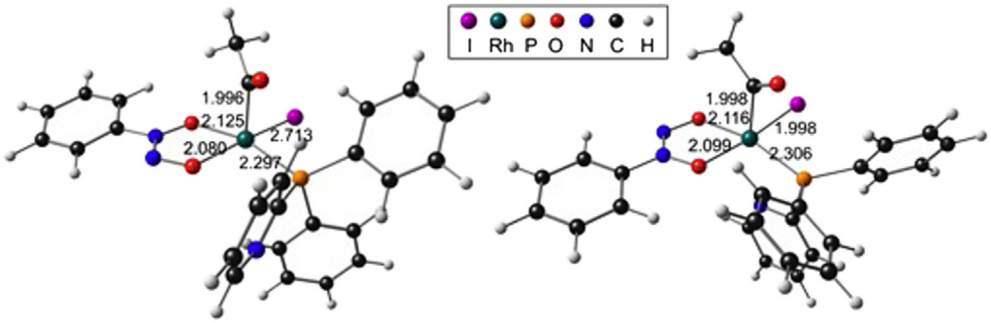

Fig. 6. ADF/PW91/TZP/acetone optimized geometry of the most stable [Rh(cupf)(DPP)($COCH_3$)(I)] acyl product isomers.

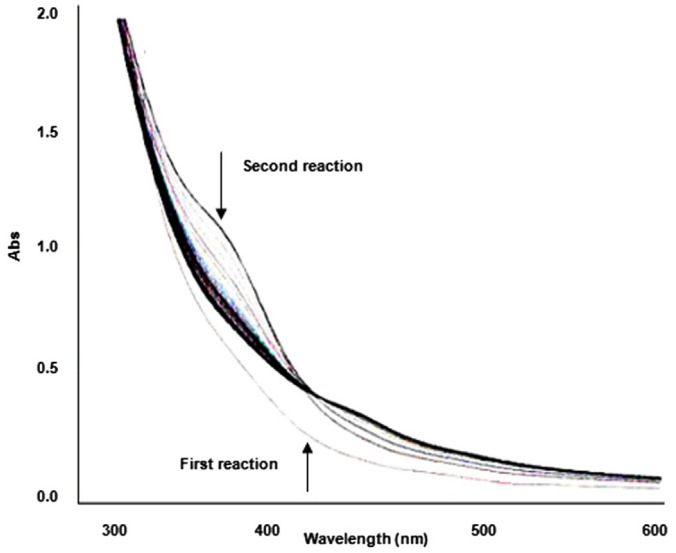

Fig. 7. Uv/vis spectra of the oxidative addition reaction of CH_3I (0.5 M) with [Rh(cupf)(CO)(DPP)] (2.5×10^{-4} M) in acetonitrile (2 min intervals, 25.0 °C).

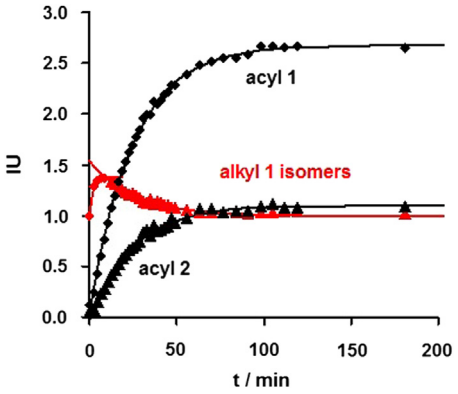

Fig. 9. Concentration-time data of the oxidative addition of CH_3I to [Rh(cupf)(CO)(DPP)] in $CDCl_3$ at 21 °C as obtained from ^1H NMR measurements. The rate decrease of the Rh(III) alkyl 1 isomers are the same as the rate of increase of the Rh(III) acyl isomers. IU = integration units of the methyl peak of the Rh(III)-complexes.

UV/visible reactions to different species formed in solution. The disappearance of the Rh(I) complex was followed by means of IR and compared to the fast reaction followed by means of UV/visible. The observed rate for the two reactions in acetonitrile (for [MeI] = 0.2 M) are 2.98×10^{-3} s^{-1} and 3.45×10^{-3} s^{-1} respectively, indicating that the fast reaction observed by the UV/visible spectra is indeed the disappearance of the Rh(I) complex or the formation of Rh(III)-alkyl complex. The [CH_3I] variation at different temperatures (Fig. 10) followed by UV/visible spectroscopy for acetonitrile indicates non-linear kinetics.

A complete [CH_3I] variation under similar conditions for IR and UV was also studied in acetone and the results also show non-linear kinetics for the first reaction. The pseudo-first-order rate constants in Table 2 confirms the excellent correlation between the fast reaction in UV/visible and the disappearance of the Rh(I) complex or the Rh(III)-alkyl formation in IR.

Non-linear kinetics results are obtained for acetonitrile, acetone and chloroform while the first reaction in ethyl acetate shows a linear correlation between k_{obs} and [CH_3I] at different temperatures (Fig. 11). These results suggest that the oxidative addition reaction between CH_3I and [Rh(cupf)(CO)(DPP)] follows the same reaction mechanism for acetonitrile, acetone and chloroform, while a different mechanism is followed in ethyl acetate.

A kinetic study of the Rh(III)-acyl formation with [CH_3I] variation at different temperatures in acetonitrile, acetone and chloroform (the second slower reaction observed on UV/vis) indicates a reaction which is independent of [CH_3I] (Fig. 12). The same reaction in ethyl acetate is, however, very slow (and not followed on UV/vis due to solvent evaporation) while the large IR absorption maximum of ethyl acetate at 1680 cm^{-1} prevents the kinetic IR monitoring of the acyl formation in ethyl acetate.

The following reaction mechanism (Scheme 1) can be constructed for three of the solvents (acetonitrile, acetone and chloroform). The mechanism postulates the rapid formation of an Rh(III)* intermediate in an equilibrium reaction followed by the formation of the Rh(III) alkyl product. In the next step, the Rh(III) alkyl product continues to react (intra molecular CO insertion or methyl migration) to form the Rh(III) acyl product.

4.3.1. Rate law for first step

The following rate law, expressed in terms of the formation of the Rh(III) intermediate, can be deducted for the oxidative addition of CH_3I to [Rh(cupf)(CO)(DPP)] in acetonitrile, acetone and chloroform as solvents

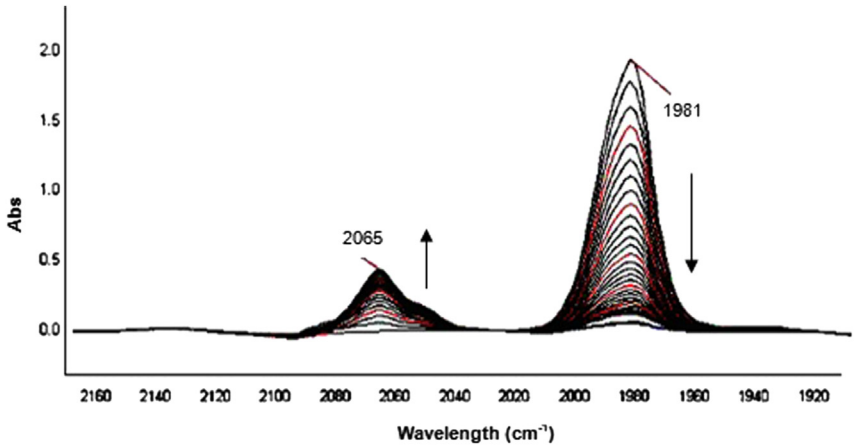

Fig. 8. IR spectra for the reaction of CH_3I (0.2 M) with [Rh(cupf)(CO)(DPP)] (2.0×10^{-2} M) in ethyl acetate (2 min intervals, 25.0 °C).

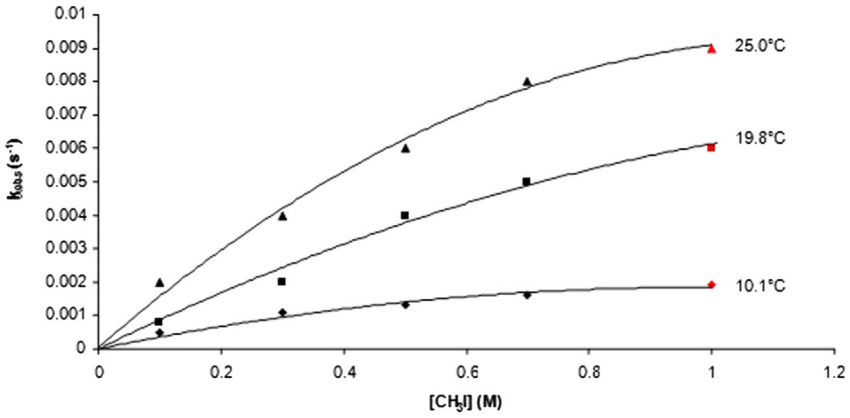

Fig. 10. k_{obs} against [CH_3I] for oxidative addition (alkyl formation) of CH_3I to [Rh(cupf)(CO)(DPP)] in acetonitrile at different temperatures as measured on the UV/vis spectrophotometer.

$$\frac{d[Rh(III)]^*}{dt} = k_1[Rh(I)][CH_3I] - k_{-1}\left[Rh(III)^*\right] - k_2[Rh(III)alkyl] \quad (2)$$

The pseudo-first-order rate constant ([CH_3I] >> [Rh(I)]) for the alkyl formation can be presented by the following:

$$k_{obs} = \frac{k_2K[CH_3I]}{1 + K[CH_3I]} \quad (3)$$

where ($K = k_1/k_{-1}$)predicts non-linear kinetics and is observed for this reaction in three of the four different solvents.

4.3.2. Rate law for second step

The rate law for the acyl product formation from the reaction scheme can be presented in the following way:

$$\frac{d[Rh(III)acyl]}{dt} = k_3[Rh(III)alkyl] \quad (4)$$

Under the prevailing experimental conditions, Equation (4) simplifies to Equation (5) (reaction is independent of [CH_3I])

$$k_{obs} = k_3 \quad (5)$$

The experimental data of the first reaction in acetonitrile, acetone and chloroform are fitted to Equation (3) and the calculated constants for the reactions at different temperatures and in different solvents are given in Fig. 13 and Table 3.

The fact that the oxidative addition reaction between CH_3I and [Rh(cupf)(CO)(DPP)] in ethyl acetate shows different spectral and much slower kinetic behavior (i.e. k_2 in Scheme 1 is in the same order as k_1), a more simplified mechanism is postulated in Scheme 2.

The rate law for the alkyl product formation from this reaction scheme can be presented in the following way:

Table 2
Comparative data for the UV and IR study for the oxidative addition reaction of CH_3I to [Rh(cupf)(CO)(DPP)] in acetone at 25 °C.

[CH_3I] (M)	UV 10^3 k_{obs} (s^{-1}) (Rh(I) disappearance or Rh(III)-alkyl formation)	IR 10^3 k_{obs} (s^{-1}) (Rh(I) disappearance)
0.1012	2.5(5)	1.57(6)
0.3021	3.6(8)	3.17(6)
0.5011	4.7(5)	4.2(5)
0.7013	5.9(5)	6.0(5)
1.016	6.3(4)	6.7(5)

$$\frac{d[Rh(I)]}{dt} = k_1[Rh(I)][CH_3I] + k_{-1}[Rh(III)alkyl] \quad (6)$$

Under pseudo-first-order conditions ([CH_3I] >> [Rh(I)]):

$$k_{obs} = k_1[CH_3I] + k_{-1} \quad (7)$$

The experimental data for ethyl acetate was fitted to Equation (7) and the calculated constants for the reaction at different temperatures are given in Table 4. The absence of any notable UV/visible spectrum change for the acyl formation reaction, the acyl/ethyl acetate IR spectral overlap as well as the slow reaction, which allows for substantial solvent loss during the reaction, prevents a thorough investigation for this reaction in ethyl acetate. It is, however, assumed that CO insertion in ethyl acetate occurs, since the acyl product is isolated from an ethyl acetate reaction mixture.

The kinetic results in Tables 3 and 4 indicate compatible alkyl formation rate constants for acetonitrile, acetone and chloroform, but a substantially slower reaction for ethyl acetate at 25 °C. These results also show little or no evidence of the influence of polarity or donocity of the different solvents on the rate of the reaction. The kinetic results show that the establishment of the equilibrium in the initial reaction (formation of Rh(I)* in Scheme 1 for chloroform, acetonitrile and chloroform) is much faster than the rate of alkyl formation as illustrated by the almost identical rate constants for the Rh(I) disappearance and the Rh(III) alkyl formation. The *K*-values of approximately one for all the solvents studied are also large enough to ensure a constant (pre-equilibrium approximation) supply of intermediate to ensure the complete disappearance of the Rh(I) monocarbonyl complex. The nature of the intermediate, as suggested by the IR and the reaction Scheme 1, is also very interesting. The direct formation of the Rh(III) peak (first at 2070 cm^{-1} and the shift to 2065 cm^{-1}) from Rh(I) as suggested by the IR, with no indication of a Rh(I) carbonyl stretching frequency shift, suggests a more loosely interaction/association between the Rh(I) center and the CH_3I molecule rather than a formal bond formation reaction. The absence of any shoulder or new peaks with the formation of the Rh(III) alkyl product in the IR study also suggests the formation of only one type of Rh(III) alkyl isomer during the first step of the reaction. The formation of this intermediate also seems to play an important role in the rate of alkyl and subsequently in acyl formation as illustrated by the much slower reactions for ethyl acetate where no evidence of any intermediate was observed. Large negative entropy of activation in all the solvents indicates an associative mechanism for the acyl formation. A slight shift in the metal (III) carbonyl stretching frequency (2004–2028 cm^{-1}) is also observed for the reaction between $[Ir_2(\mu\text{-Dcbp})(CO)_2(PCy_3)_2]^-$ and CH_3I [45], but this is also accompanied by a shift in Ir(I) carbonyl

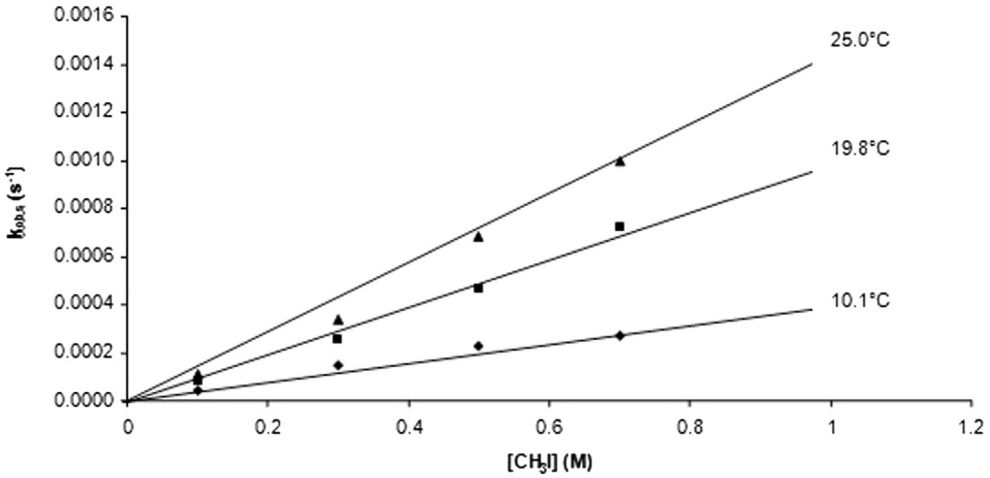

Fig. 11. k_{obs} against [CH_3I] for oxidative addition (alkyl formation) of CH_3I to [Rh(cupf)(CO)(DPP)] in ethyl acetate different temperatures as measured on the UV/vis spectrophotometer.

stretching frequency, attributed to the presence of two different Ir species in the complex.

A comparison of the rate constants of the current study with that of other [Rh(cupf)(CO)(PX_3)] complexes is summarized in Table 5. This comparative study allows for the isolation of the steric or the electronic influence of the different phosphine ligands on the rate of alkyl and acyl formation. For this comparison, the cone angle for the DPP was estimated to be the same as that for PPh_3 (145°) as the only difference between the two ligands is the pyridyl-ring for DPP compared to the normal phenyl ring for PPh_3. The results in Table 5 clearly indicate that the cone angle for the first four phosphine groups are the same, however an increase of a factor of 50 (from P(*p*-ClC_6H_4)$_3$ to DPP) was observed for the rate of Rh(III) alkyl formation and a factor 8 increase in Rh(III) acyl formation, with the faster reaction for the electron rich DPP. The increase in oxidative addition rate as well as acyl formation can be attributed to the electronic parameter or electron donating property of the DPP ligand. It is therefore anticipated that the additional electron density of this phosphine increases the nucleophilicity of the metal center which subsequently increase the reaction rate with the CH_3I molecule.

The apparent discrepancies in the rates of oxidative addition and mechanisms for the different solvents for the oxidative addition of CH_3I to [Rh(cupf)(CO)(DPP)] prompted a DFT study to gain more insight into this reaction, as well as to try and determine the geometry of the transition state as predicted in Scheme 1.

4.4. DFT study of the oxidative addition reaction

It is widely accepted that the S_N2 oxidative addition of simple substrates such as MeI, to square planar complexes occurs via a stepwise mechanism (Scheme 3). The first step is nucleophilic substitution of iodide by the metal complex, presumed to proceed with *inversion* of configuration at the carbon atom. The substitution of iodide by the metal complex and the simultaneous expulsion of an iodide ion lead to the formation of a five-coordinated species. Subsequent coordination of iodide to the free coordination site of the complex completes the addition to give a six-coordinate alkyl complex. A wealth of kinetic, stereochemical, and spectroscopic data support this mechanism. Two S_N2 processes have been reported for the *trans* addition, the "linear/back" and the "bent" TS, see Scheme 4 [49]. The linear/back transition state structure corresponds to an S_N2 mechanism, characterized by a linear Rh-C_{methyl}-I arrangement and by an Rh-C_{methyl}-H angle close to 90°. The methyl hydrogen atoms are located in the equatorial plane of the five-coordinated carbon atom, resulting in a trigonal bipyramidal arrangement. The bent transition state structure corresponds to a side-on approach of the C_{methyl}-I bond to the rhodium atom (Scheme 4). The bent transition state structure leads to the same intermediate product as the linear/back transition state structure, namely a cationic five-coordinated rhodium complex and a free iodide ion. Another pathway, which has been considered, is concerted *cis* or front addition and is expected to lead to the

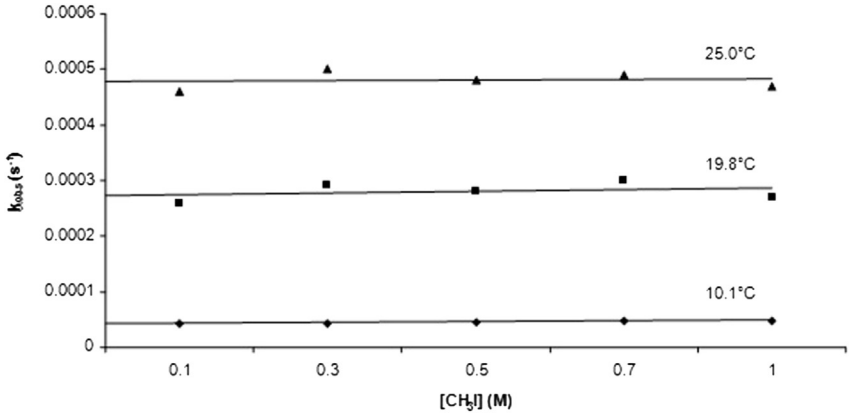

Fig. 12. k_{obs} against [CH_3I] for insertion reaction (acyl formation) in acetonitrile at different temperatures as measured on the UV/vis spectrophotometer.

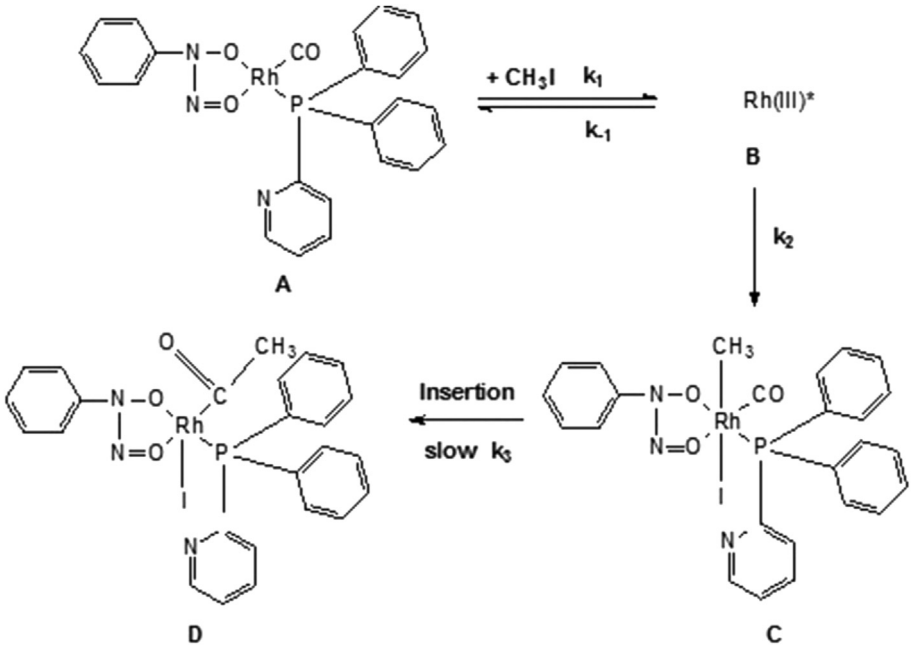

Scheme 1. Proposed mechanism for the oxidative addition of CH_3I and [Rh(cupf)(CO)(DPP)] in acetone, acetonitrile and chloroform with k_1 step fast, k_2 step slow and, k_3 very slow.

retention of configuration at carbon [49]. In the front transition state structure the Rh—I and Rh-C_{methyl} bonds form simultaneously as I-C_{methyl} bond breaks, resulting in the *cis* addition of the methyl iodide (Scheme 4).

The activation energy (E_{act}) for the linear, bent and front (*cis*) TS calculated in this study for the title compound is given in Table 1 and from these results it is clear that the linear TS is energetically favored. The geometry of the "linear" TS of the [Rh(cupf)(DPP)(CO)] + CH_3I reaction for both isomers in acetone solvent is illustrated in Fig. 14. The TS involves the classical backside attack by the rhodium nucleophile, leading to inversion of stereochemistry at carbon. Both TS structures correspond to a S_N2-like approach characterized by a near linear I—CH_3—Rh arrangement and by an I—CH_3—H angle close to 90°. The methyl hydrogen atoms are located in the equatorial plane of the five-coordinated carbon atom, showing the expected trigonal bipyramidal geometry. This kind of structure has been characterized in a number of related cases [50,51] and was first proposed by Griffin et al. [49]. In the TS structures the Rh—C and C—I distances agree with a concerted formation of the Rh—C bond and a rupture of the C—I bond. The imaginary frequency (−313 and −303 for addition to isomers A and B, respectively) of the TS corresponds to a CH_3I stretching vibrational mode in which the I—C_{CH3} bond breaks and the Rh—C_{CH3} bond forms.

The formation of the TS is followed by the formation of the cationic five-coordinate $[Rh(cupf)(CO)(DPP)(CH_3)]^+$ intermediate (IM) with the CH_3 group in the apical position and with the iodide ion drifting away into the solvent sphere (Fig. 14). The relative energy of the intermediate is 0.14 eV (13 kJ mol^{-1}) less than that of the transition state. The free iodide then coordinates to the rhodium center to form the *trans* rhodium(III) alkyl oxidative addition product with a final Rh—I bond length of 2.94 Å and energy of 0.5 eV (48 kJ mol^{-1}) lower than the intermediate in acetone as solvent (Fig. 4). In the next step, an inversion of the configuration of hydrogen at the methyl carbon occurred and the methyl group is fully bonded to the rhodium atom.

The calculated activation energy (E_a in Table 1) or the calculated activation Gibbs energy (ΔG^* in Table 6) of the front transition state leading to alkyl 2a of Fig. 15, is *ca*. four and two times higher than the calculated values leading to alkyl 1a and 2a, respectively. This

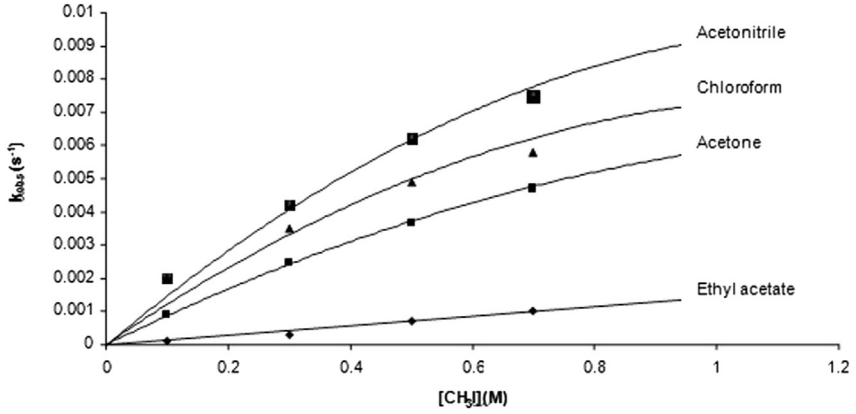

Fig. 13. k_{obs} against [CH_3I] for oxidative addition (alkyl formation) of CH_3I to [Rh(cupf)(CO)(DPP)] in different solvents at 25 °C as measured on the UV/vis spectrophotometer.

Table 3
Summary for the oxidative addition of CH_3I to [Rh(cupf)(CO)(DPP)] at different temperatures in acetonitrile, acetone and chloroform as obtained from UV/vis measurements.

Solvent	Temp (°C)	10^3 k_2 (alkyl) ($M^{-1}s^{-1}$)	10^3 k_3(acyl) (s^{-1})	K (M^{-1})	ΔH* ($kJ.mol^{-1}$)	ΔS* ($J.K^{-1}.mol^{-1}$)
Acetonitrile	10.1	5.0(1)	0.043(5)	1.99(1)	48(9)	-214(7)
	19.8	7.0(2)	0.29(6)	0.2(1)		
	25.0	17(6)	0.49(6)	0.9(1)		
Acetone	10.1	3.0(2)	0.044(5)	1.7(4)	34(8)	-209(6)
	19.8	8.0(2)	0.039(6)	1.4(1)		
	25.0	9.0(1)	1.1(5)	0.5(1)		
Chloroform	10.1	1.4(4)	0.11(7)	0.39(2)	12(9)	-173(7)
	19.8	13.4(2)	0.59(6)	4.6(9)		
	25.0	20(3)	1.1(5)	2.6(4)		

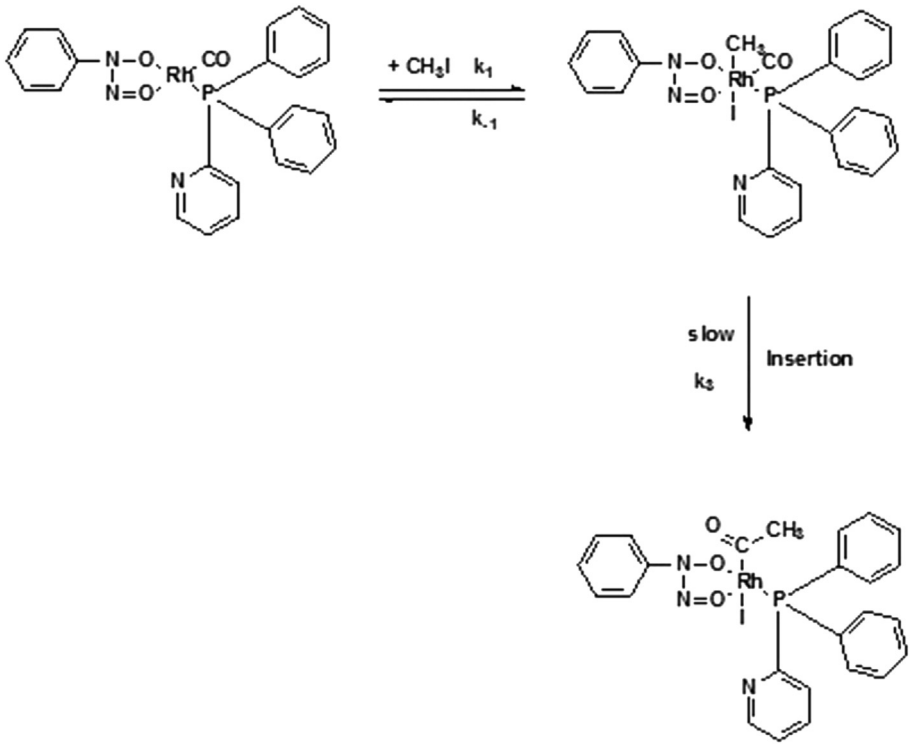

Scheme 2. Proposed mechanism for the oxidative addition of CH_3I and [Rh(cupf)(CO)(DPP)] in ethyl acetate.

Table 4
Summary for the oxidative addition of CH_3I to [Rh(cupf)(CO)(DPP)] at different temperatures in ethyl acetate as obtained from UV/vis measurements.

Temperature (°C)	10^3 k_1 ($M^{-1}s^{-1}$)	10^4 k_{-1} (s^{-1})	K (M^{-1})	ΔH* ($kJ.mol^{-1}$)	ΔS* ($J.K^{-1}.mol^{-1}$)
10.1	0.12(2)	0.60(1)	2.0(2)	19(9)	-238(8)
19.8	1.03(3)	0.39(2)	2.64(1)		
25.0	1.59(7)	0.98(4)	1.62(2)		

Table 5
Rate constants for the oxidative addition of CH_3I to different [Rh(cupf)(CO)(PX_3)] complexes in acetone at 25 °C.

PX_3	Cone angle/θ	Tolman electronic parameter/ν (cm^{-1})	pK_a	10^3k (alkyl) (M^{-1} s^{-1})	10^3k (acyl)(s^{-1})	Reference
P(*p*-ClC_6H_4)$_3$	145	2072.8	1.03	0.193(8)	0.14(6)	[46,47]
PPh_3	145	2068.9	2.73	1.22(2)	0.31(1)	[46,47]
P(*p*-$MeOC_6H_4$)$_3$	145	2066.1	4.57	4.20(8)	0.20(5)	[46,47]
DPP	~145[#]	2066.7[a]	4.07	9.0(1)	1.1(5)	This study, [45,48]
PCy_3	170	2056.4	9.65	1.94(3)	0.24(2)	[46,47]

[a] Calcultated value according to Tolman eq.. $\upsilon_{CO}(A_1) = 2056.1 + \sum_{i=1}^{3} \chi_i cm^{-1}$.

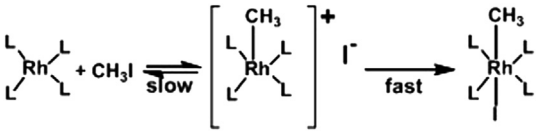

Scheme 3. The widely accepted two step S_N2 mechanism for the oxidative addition of iodomethane to square planar rhodium complexes.

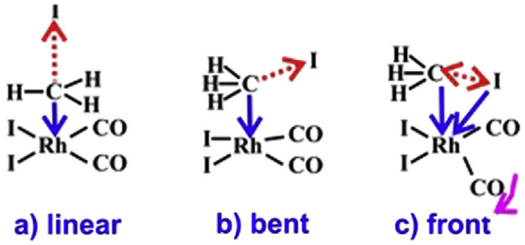

Scheme 4. Schematic illustration of a "linear/back", "bent" and "front/concerted cis" transition states of the nucleophilic attack of square planar rhodium(I) on methyl iodide. The Monsanto catalyst $[Rh(CO)_2I_2]^-$ is used as example for the square planar rhodium(I) complex. The solid arrows indicate bond formation, the dotted arrows bond breaking and the curved arrow the movement of CO.

result is in agreement with *trans* addition of iodomethane to [Rh(cupf)(CO)(DPP)] leading to the formation of two trans alkyl product isomers (alkyl 1a and 2a).

The activation parameters of the linear and selected front transition states were calculated for the solvents used in this study and compared to the experimentally obtained values in Table 6. The best agreement between experimental and calculated values is obtained for the linear transition state, whereas the calculated values for the front transition state do not match the experimental values. The good agreement between the experimental and calculated values obtained for acetone and ethyl acetate as solvent, highlight the fact that the oxidative addition reaction in both solvents follows the same reaction path. The properties and the geometry of the calculated TS in the different solvents were found to be very similar. The activation energy and relative energies of the ionic intermediate and alkyl 1 product, are also very similar (Table 1). The calculated results do not show a significant difference in the mechanism of the first oxidative addition step of the [Rh(cupf)(CO)(DPP)] + CH_3I reaction in different solvents. The experimentally observed difference in the mechanisms of the [Rh(cupf)(CO)(DPP)] + CH_3I reaction in ethyl acetate relative to the other solvents studies, can thus not be explained by the computational chemistry results of this study.

The experimentally observed difference in the mechanisms of the [Rh(cupf)(CO)(DPP)] + CH_3I reaction in ethyl acetate relative to the other solvents studies, is thus most probably due to the rate of formation of the TS (k_1 step in Scheme 1) and/or the build-up and conversion of the IM in the different solvents which led to the substantial difference in the rate of alkyl formation in the two sets of solvents.

5. Conclusion

This comparative study highlighted the complexity of factors that ultimately influence or control the rate of oxidative addition and finally acyl formation. The substitution of a phoshine's phenyl ring with a pyridyl group results in an increase in oxidative addition rate for [Rh(cupf)(CO)(DPP)] in excess of an order of magnitude relative to other [Rh(cupf)(CO)(PR_3)] complexes, PR_3 = tertiary phosphine. A change in solvent does not only play an important

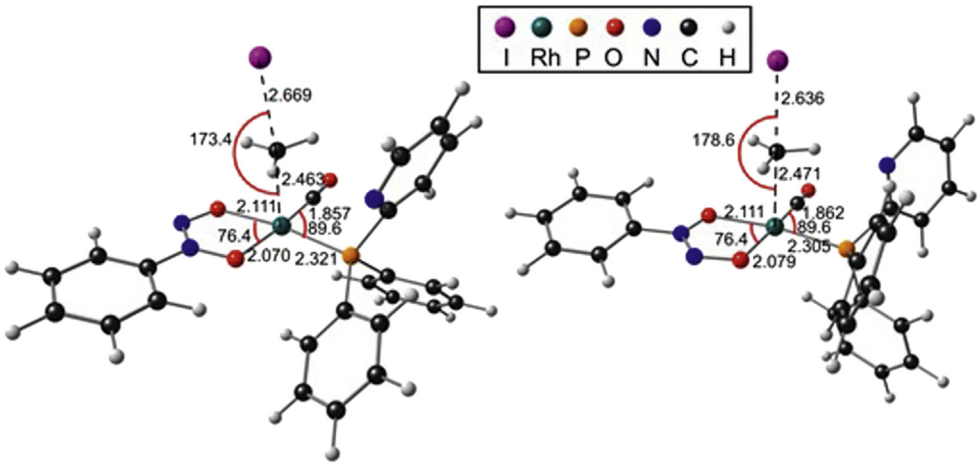

Fig. 14. ADF/PW91/TZP/acetone optimized geometry of the linear TS of the [Rh(cupf)(DPP)(CO)] + CH_3I reaction. Left is the TS of the oxidative addition to isomer A and right to isomer B.

Table 6
Experimental and ADF/PW91 calculated activation parameters of the [Rh(cupf)(CO)(DPP)] + CH_3I reaction in different solvents.

		Trans addition (linear TS)			Cis addition (front TS)		
		ΔH^*/(kJ mol^{-1})	ΔS^*/(J K^{-1} mol^{-1})	ΔG^*/(kJ mol^{-1})	ΔH^*/(kJ mol^{-1})	ΔS^*/(J K^{-1} mol^{-1})	ΔG^*/(kJ mol^{-1})
Ethyl acetate	Experimental	19(9)	−238(8)	90			
	Calc. isomer A + CH_3I	25	−230	94	102	−221	167
	Calc. isomer B + CH_3I	30	−175	83			
Acetone	Experimental	34(8)	−209(6)	96			
	Calc. isomer A + CH_3I	30	−177	83	110	−145	153
	Calc. isomer B + CH_3I	31	−150	76			
Chloroform	Experimental	12(9)	−173(7)	64			
	Calc. isomer A + CH_3I	29	−204	90	104	−194	162
	Calc. isomer B + CH_3I	22	−249	97			
Acetonitrile	Experimental	48(9)	−214(7)	112			
	Calc. isomer A + CH_3I	26	−200	86	108	−170	159
	Calc. isomer B + CH_3I	24	−225	91			
Methanol	Calc. isomer A + CH_3I	26	−221	91	113	−137	154
	Calc. isomer B + CH_3I	32	−151	77			

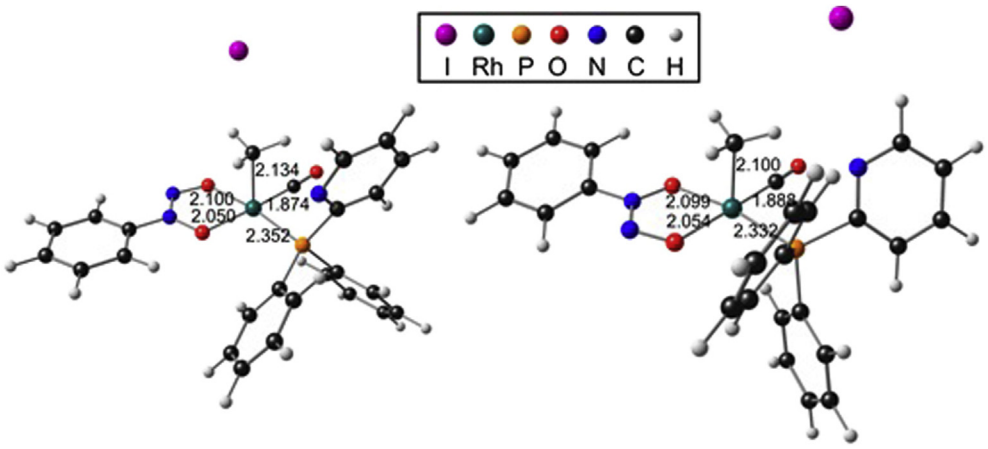

Fig. 15. ADF/PW91/TZP/acetone optimized geometry of the cationic five-coordinate [Rh(cupf)(CO)(DPP)(CH_3)]$^+$ intermediate (IM). Left is the IM of the oxidative addition to isomer A and right to isomer B.

role in the rate of the reaction, but also on the type of reactive species that can experimentally be observed during the reaction sequence. Results from a DFT study do not show any difference in the mechanism of the first oxidative addition step of the [Rh(cupf)(CO)(DPP)] + CH_3I reaction in different solvents. The experimentally observed difference in the rates and mechanisms of the [Rh(cupf)(CO)(DPP)] + CH_3I reaction in ethyl acetate relative to the other solvents studied, can most probably be attributed to the rate of the formation and/or the build-up of the IM as well as the rate of the alkyl 1 formation.

Acknowledgments

The authors thank the Research Fund of this University and the National Research Foundation of the Republic of South Africa for financial support.

References

[1] J. Hagen, Industrial Catalysis, a Practical Approach, second ed., Wiley VCH, Weinheim, 2006, pp. 425–427.
[2] S. Scott, Canadian Chemical News, 1999. www.allbusiness.com/north-america/Canada/ (accessed 18.03.10).
[3] H. Kidwell, www.in-pharmatechnologist.com/content/, 29 January 2008 (accessed 16.03.10).
[4] Platinum Today, Johnson Matthey, 2004 (accessed 16.03.10).
[5] CORDIS.Europe.eu., 2006 (accessed 18.03.10).
[6] A. Haynes, P.M. Maitlis, G.E. Morris, G.J. Sunley, H. Adams, P.W. Badger, C.M. Bowers, D.B. Cook, P.I.P. Elliot, T. Ghaffar, H. Green, T.R. Griffin, M. Payne, J.-M. Pearson, M.J. Taylor, P.W. Vickers, R.J. Watt, J. Am. Chem. Soc. 126 (2004) 2847–2861, http://dx.doi.org/10.1021/ja039464y.
[7] T.W. Dekleva, D. Foster, Adv. Catal. 34 (1986) 81–130, http://dx.doi.org/10.1016/S0360-0564(08)60591-X.
[8] (a) P.M. Maitlis, A. Haynes, G.J. Sunley, M.J. Howard, J. Chem. Soc. Dalton Trans. (1996) 2187–2196, http://dx.doi.org/10.1039/DT9960002187;
(b) A. Hayes, B.E. Mann, D.J. Gulliver, G.E. Morris, P.M. Maitlis, Am. Chem. Soc. 113 (1991) 8567–8569, http://dx.doi.org/10.1021/ja00022a079.
[9] NIST Advanced Technology Programme on Catalysis and Biocatalysis, White Paper: Leveraging Resources and Targeting Performance, 1998.
[10] (a) S.S. Basson, J.G. Leipoldt, J.T. Nel, Inorg. Chim. Acta 86 (1984) 167–172;
(b) S.S. Basson, J.G. Leipoldt, A. Roodt, J.A. Venter, T.J. van der Walt, Inorg. Chim. Acta 119 (1986) 35–38, http://dx.doi.org/10.1016/S0020-1693(00)81327-4;
(c) S.S. Basson, J.G. Leipoldt, A. Roodt, J.A. Venter, Inorg. Chim. Acta 128 (1987) 31–37, http://dx.doi.org/10.1016/S0020-1693(00)84691-5;
(d) J.G. Leipoldt, S.S. Basson, L.J. Botha, Inorg. Chim. Acta 168 (1990) 215–220, http://dx.doi.org/10.1016/S0020-1693(00)80945-7;
(e) J.G. Leipoldt, E.C. Steynberg, R. van Eldik, Inorg. Chem. 26 (1987) 3068–3070, http://dx.doi.org/10.1021/ic00265a029;
(f) G.J. van Zyl, G.J. Lamprecht, J.G. Leipoldt, T.W. Swaddle, Inorg. Chim. Acta 143 (1988) 223–227, http://dx.doi.org/10.1016/S0020-1693(00)83693-2;
(g) J.G. Leipoldt, G.J. Lamprecht, G.J. van Zyl, Inorg. Chim. Acta 96 (1985) L31–L34, http://dx.doi.org/10.1016/S0020-1693(00)93728-9;
(h) D.M.C. Smit, S.S. Basson, A. Roodt, E.C. Steynberg, Rhodium Express 7 and 8 (1994) 12–16;
(i) Y.M. Terblans, S.S. Basson, W. Purcell, G.J. Lamprecht, Acta Crystallogr. C51 (1995) 1748–1750, http://dx.doi.org/10.1107/S010827019500254X;
(j) P. Ebenebe, S.S. Basson, W. Purcell, Rhodium Express 16 (1996) 11–16;
(k) M. Theron, E. Grobbelaar, W. Purcell, S.S. Basson, Inorg. Chim. Acta 358 (2005) 2457–2463, http://dx.doi.org/10.1016/j.ica.2004.06.070;
(l) E. Grobbelaar, W. Purcell, S.S. Basson, Inorg. Chim. Acta 359 (2006) 3800–

3806, http://dx.doi.org/10.1016/j.ica.2006.03.041;
(m) J. Conradie, G.J. Lamprecht, A. Roodt, J.C. Swarts, Polyhedron. 26 (2007) 5075–5087, http://dx.doi.org/10.1016/j.bbr.2011.03.031;
(n) M.M. Conradie, J. Conradie, Inorg. Chim. Acta 361 (2008) 2285–2295, http://dx.doi.org/10.1016/j.ica.2007.10.052;
(o) J. Conradie, J.C. Swarts, Organometallics 28 (2009) 1018–1026, http://dx.doi.org/10.1021/om800655j;
(p) A.J. Muller, J. Conradie, W. Purcell, S.S. Basson, J.A. Venter, S. Afr. J. Chem. 63 (2010) 11–19.

[11] (a) N.W. Alcock, P. Moore, P.A. Lampe, K.F. Mok, J. Chem. Soc. Dalton Trans. (1982) 207–210, http://dx.doi.org/10.1039/DT9820000207;
(b) M.M. Olmstead, A. Maisonhat, J.P. Farr, A.L. Balch, Inorg. Chem. 20 (1981) 4060–4064, http://dx.doi.org/10.1021/ic50226a005;
(c) Y. Inoguchi, B. Milewski-Mahrla, H. Schmidbauer, Chem. Ber. 115 (1982) 3085–3095, http://dx.doi.org/10.1002/cber.19821150914;
(d) H.J. Wasserman, D.C. Moody, R.T. Paine, R.R. Ryan, K.V. Salazar, J. Chem. Soc. Chem. Commun. (1984) 533–534.

[12] (a) U. Abram, R. Alberto, J.R. Dilworth, Y. Zheng, K. Ortner, Polyhedron. 18 (1999) 2995–3003, http://dx.doi.org/10.1016/S0277-5387(99)00216-8;
(b) P. Govindaswamy, P.J. Carroll, Y.A. Mozharivskyj, M.R. Kollipara, J. Chem. Sci. 118 (2006) 319–326, http://dx.doi.org/10.1007/BF02708525;
(c) J.P. Farr, M.M. Olmstead, F.E. Wood, A.L. Balch, J. Am. Chem. Soc. 105 (1983) 792–798, http://dx.doi.org/10.1021/ja00342a024.

[13] T.T. Chiweshe, W. Purcell, J.A. Venter, S. Afr. J. Chem. 66 (2012) 7–16.

[14] Scientist, Version 2, MicroMath Scientific Software, Saint Louis, Mo, 2004.

[15] A. Rusina, A.A. Vlček, Nature 206 (1965) 295–296, http://dx.doi.org/10.1038/206295a0.

[16] G. te Velde, F.M. Bickelhaupt, E.J. Baerends, C. Fonseca Guerra, S.J.A. van Gisbergen, J.G. Snijders, T. Ziegler, J. Comput. Chem. 22 (2001) 931–967, http://dx.doi.org/10.1002/jcc.1056.

[17] C. Fonseca Guerra, J.G. Snijders, G. te Velde, E.J. Baerends, Theor. Chem. Acc. 99 (1998) 391–403, http://dx.doi.org/10.1007/s002140050353.

[18] ADF2009.01, SCM, Theoretical Chemistry, Vrije Universiteit, Amsterdam, The Netherlands.

[19] (a) J.P. Perdew, J.A. Chevary, S.H. Vosko, K.A. Jackson, M.R. Pederson, D.J. Singh, C. Fiolhais, Phys. Rev. B 46 (1992) 6671–6687, http://dx.doi.org/10.1103/PhysRevB.46.6671;
(b) J.P. Perdew, J.A. Chevary, S.H. Vosko, K.A. Jackson, M.R. Perderson, D.J. Singh, C. Fiolhais, Phys. Rev. B 48 (1993) 4978, http://dx.doi.org/10.1103/PhysRevB.48.4978.2.

[20] L. Fan, T. Ziegler, J. Chem. Phys. 96 (1992) 9005–9012, http://dx.doi.org/10.1063/1.462258.

[21] L. Fan, T. Ziegler, J. Amer. Chem. Soc. 114 (1992) 10890–10897, http://dx.doi.org/10.1021/ja00053a027.

[22] J.H. Espenson, Chemical Kinetics and Reaction Mechanisms, second ed., 15„ McGraw-Hill, New York, 1995, 49, 70–75, 156.

[23] A. Klamt, G. Schüürmann, J. Chem. Soc. Perkin Trans. 2 (1993) 799–805, http://dx.doi.org/10.1039/P29930000799.

[24] A. Klamt, J. Phys. Chem. 99 (1995) 2224–2235, http://dx.doi.org/10.1021/j100007a062.

[25] A. Klamt, V. Jones, J. Chem. Phys. 105 (1996) 9972–9981, http://dx.doi.org/10.1063/1.472829.

[26] C.C. Pye, T. Ziegler, Theor. Chem. Acc. 101 (1999) 396–408, http://dx.doi.org/10.1007/s002140050457.

[27] J.L. Pascual-Ahuir, E. Silla, I. Tuñon, J. Comput. Chem. 15 (1994) 1127–1138, http://dx.doi.org/10.1002/jcc.540151009.

[28] http://www.chemicalize.org/structure/#!mol=diphenyl-2-pyridylphosphine (accessed 27.10.11).

[29] S.S. Basson, J.G. Leipoldt, A. Roodt, J.A. Venter, Inorg. Chim. Acta 118 (1986) 45–46.

[30] W. Purcell, J. Conradie, T.T. Chiweshe, J.A. Venter, H.G. Visser, M.P. Coetzee, J. Mol. Struct. 1038 (2013) 220–229, http://dx.doi.org/10.1016/j.molstruc.2013.01.061.

[31] J.J.C. Erasmus, M.M. Conradie, J. Conradie, React. Kinet. Mech. Catal. 105 (2012) 233–247, http://dx.doi.org/10.1007/s11144-011-0413-1.

[32] M.M. Conradie, J. Conradie, Inorg. Chim. Acta 361 (2008) 208–218, http://dx.doi.org/10.1016/j.ica.2007.07.010.

[33] M.M. Conradie, J. Conradie, S. Afr. J. Chem. 61 (2008) 102–111.

[34] J. Conradie, G.J. Lamprecht, S. Otto, J.C. Swarts, Inorg. Chim. Acta 328 (2002) 191–203, http://dx.doi.org/10.1016/S0020-1693(01)00731-9.

[35] K.H. Hopmann, N.F. Stuurman, A. Muller, J. Conradie, Organometallics 29 (2010) 2446–2458, http://dx.doi.org/10.1021/om1000138.

[36] N.F. Stuurman, J. Conradie, J. Organomet. Chem. 694 (2009) 259–268, http://dx.doi.org/10.1016/j.jorganchem.2008.10.040.

[37] A.M.M. Trzeciak, J.J. Ziólkowsk, Inorg. Chim. Acta 96 (1985) 15–20, http://dx.doi.org/10.1016/S0020-1693(00)93731-9.

[38] W. Purcell, S.S. Basson, J.G. Leipoldt, A. Roodt, H. Preston, Inorg. Chim. Acta 234 (1995) 153–156, http://dx.doi.org/10.1016/0020-1693(95)04469-P.

[39] N.F. Stuurman, A. Muller, J. Conradie, Inorg. Chim. Acta 395 (2013) 237–244, http://dx.doi.org/10.1016/j.ica.2012.11.001.

[40] M.M. Conradie, J. Conradie, Inorg. Chim. Acta 362 (2009) 519–530, http://dx.doi.org/10.1016/j.ica.2008.04.046.

[41] M.M. Conradie, J. Conradie, Dalton Trans. 40 (2011) 8226–8237, http://dx.doi.org/10.1039/C1DT10271K.

[42] M.M. Conradie, J. Conradie, J. Organomet. Chem. 695 (2010) 2126–2133, http://dx.doi.org/10.1016/j.jorganchem.2010.05.021.

[43] Cambridge Structural Database (CSD). Version 5, 2010, p. 32.

[44] J.A. Venter, W. Purcell, H.G. Visser, Acta Crystallogr. E65 (2009) m1528–m1529, http://dx.doi.org/10.1107/S1600536809043050.

[45] E. Grobbelaar, J. Conradie, W. Purcell, J.A. Venter, W. Purcell, T.T. Chiweshe, J. Organomet. Chem. 696 (2011) 1990–2002, http://dx.doi.org/10.1016/j.jorganchem.2010.10.049.

[46] D.E. Graham, G.J. Lamprecht, I.M. Potgieter, A. Roodt, J.G. Leipoldt, Transit. Met. Chem. 16 (1991) 193–195.

[47] C.A. Tolman, Chem. Rev. 77 (1977) 313–348, http://dx.doi.org/10.1021/cr60307a002.

[48] C.A. Tolman, J. Am. Chem. Soc. 92 (1970) 2953–2956, http://dx.doi.org/10.1021/ja00713a007.

[49] T.R. Griffin, D.B. Cook, A. Haynes, J.M. Pearson, D. Monti, G.E. Morris, J. Am. Chem. Soc. 118 (1996) 3029–3030, http://dx.doi.org/10.1021/ja952952o.

[50] B. Bogdanov, T.B. McMahon, Int. J. Mass Spectrom. 241 (2005) 205–223, http://dx.doi.org/10.1016/j.ijms.2004.12.018.

[51] M. Feliz, Z. Freixa, P.W.N.M. van Leeuwen, C. Bo, Organometallics 24 (2005) 5718–5723, http://dx.doi.org/10.1021/om050554g.